Volume 1 | Number 1 | Jan 2013 | Pages 1–100

Journal of
Materials Chemistry B

Materials for biology and medicine
www.rsc.org/materialsB

ROYAL SOCIETY
OF CHEMISTRY

ROYAL SOCIETY
OF CHEMISTRY

www.rsc.org/materialsB

Journal Materials Chemistry B

PAPER

Engineered ECM-like microenvironment with fibrous particles for guiding 3D-encapsulated hMSC behaviours

Young Min Shin,[a] Taek Gyoung Kim,[b] Jong-Seok Park,[a] Hui-Jeong Gwon,[a] Sung In Jeong,[a] Heungsoo Shin,[c] Kyung-Soo Kim,[d] Myung-Han Yoon,[e] and Youn-Mook Lim[a]*

Alginate hydrogel has been used as an attractive scaffold for tissue regeneration. In particular, its simple cross-linking, high water absorption, and biocompatibility have provided its utility in regulating an interaction with cells or organs. However, three-dimensional (3D) networks of alginate hydrogel do not provide fibrous anchorage sites such as the collagen fibres in natural extracellular matrix (ECM). This has partially limited the survival of anchorage-dependent cells in the 3D hydrogel environment. In this report, we established a hybrid hydrogel containing fibrous particles (FP) that closely mimics the ECM. The RGD peptide-coupled FP (R-FP) has a wide length of distribution and was homogeneously dispersed in the hydrogel. The encapsulated human mesenchymal stem cells in the hydrogel could bind to the R-FP presenting remarkable spreading morphology, augmented viability and differentiation. These findings may elicit the significance of a physical interaction in which R-FP provides structural and biological cues to the cells. This strategy can be widely applicable to a variety of hydrogel systems.

Introduction

Hydrogel has been widely used as a cell delivery carrier or 3-dimensional (3D) scaffold in the fields of tissue engineering and regenerative medicine. Its inter-connected network structure, higher water absorption and biocompatibility allow for its easy generation of a cell-compatible microenvironment.[1] Among the raw materials used for hydrogels, alginate is the most popular due to easy cross-linking by Ca^{2+}, Mg^{2+}, and Ba^{2+} ions and its biocompatibility.[2-4] The cross-linked alginate hydrogel provides a favourable microenvironment for cell survival, which has been used in cartilage tissue engineering and regulation of human mesenchymal stem cells (hMSC) behaviours.[5,6] However, pristine alginate hydrogel often fails to provide cell-interactive cues that allow for cell adhesion and survival on the surface or inside the hydrogel, which consequently results in poor cell survival for a long-time culture. To overcome this limitation of the alginate hydrogel, numerous efforts have been made to enhance its cellular interacting ability by conjugation of cell-binding peptides or incorporation of extracellular matrix (ECM) proteins.[7,8] For example, arginine-glycine-aspartic acid (RGD), a peptide derived from fibronectin or collagen, was bound to the alginate backbone through 1-ethyl-3-(3-dimethylaminopropyl)-carbodiimide (EDC) chemistry.[9] Gelatin and collagen have also been mixed in the alginate to develop more biocompatible hydrogels.[10,11] Those modified hydrogels successfully improved viability and protein expression of hMSC, osteoblast, cardiac cells, and fibroblasts.[12-15]

Although the chemical modification of raw materials or addition of cell-interactive proteins to the hydrogel has provided a method for delivering cell-interactive moieties,[16] huge structural differences still remain between the microenvironments of artificial hydrogel and the natural ECM. For example, collagen and elastin forms a fibrous structure of nano to micro-scale range in the ECM.[17] They have played their own fundamental roles, such as providing many cell anchorage sites or assembling with other cell binding proteins, in order to regulate complex intrinsic signal transduction.[18] However, current biomolecule-modified hydrogels only provide a dense polymeric chain network, and they do not offer the fibrous architecture as seen in the natural ECM. Because it is well-known that most anchorage-dependent cells should be attached on the stiff surface (polystyrene tissue culture plate) for increased survival,[19] their recognition of the adhesion sites should be significant in regulating further survival.

ECM-like fibrous architecture has been mimicked through an electrospinning method.[20] It not only generated random or aligned fibrous meshes, but it also produced meshes with nano- to micron fibre diameter.[21,22] However, most of the electrospun nanofibers have relatively small pores that restrict cell infiltration into the nanofibers. Furthermore, 3D scaffolding function has only partially been achieved.[23, 24] To overcome the limitations of nanofiber mesh, we report a fragmented fibre prepared by aminolysis and shear stress,[25] and we suggest a new approach for cell delivery using the spheroid of the fragmented fibre and hMSC in a polycaprolactone (PCL) scaffold.[26] The fragmented fibres can be well dispersed in the solution, and its size is relatively larger than that of common spherical nanoparticles, which provides low cytotoxicity without intracellular uptake. Furthermore, because it can provide collagen-like cell binding sites due to the conjugated RGD peptide, the incorporation of the fragmented fibres in the hydrogel may closely mimic the ECM structure, and it can be considered as an alternative additive to a variety of hydrogels requiring chemical modification.

In this study, we establish a hybrid hydrogel containing fragmented fibres (referred to as fibrous particles, FP) as a biomimetic 3D microenvironment. We hypothesized that the incorporation of RGD peptide-conjugated FP within the alginate hydrogels can regulate 3D-encapsulated hMSC survival by providing a fibrous anchorage site as well as a cell adhesive ligand. To test our hypothesis, the FP was prepared by aminolysis of electrospun poly(L-lactide) (PLLA) mesh, and the RGD peptide was immobilized on the FP through EDC chemistry after acrylic acid (AAc)-grafting by γ-ray irradiation. We subsequently investigated hMSC behaviour in the hybrid hydrogel.

Experimental

Materials

Materials utilized in this study were obtained as follows: Poly(L-lactide) (PLLA, Resomer® L214S) from Evonic Industries (Essen, Germany), Dulbecco's modified eagle's medium (DMEM) and foetal bovine serum (FBS) from Gibco (Grand Island, NY, USA), trifluoroethanol (TFE) and hexamethylenediamine (HMDA) from Sigma (St. Louis, MO, USA), and dichloromethane (DCM) from Junsei (Tokyo, Japan). The fluorescent probes rhodamine-phalloidin, Hoechst 33258, and Alexa Fluor 488 rabbit anti-mouse IgG were obtained from Molecular Probes (Eugene, OR, USA), and a Milli-Q Plus System (Millipore, Billerica, MA, USA) was used to produce ultrapure water. All other chemicals and solvents were of analytical grade and were used without further purification.

Fabrication of electrospun nanofibrous meshes

PLLA (3 wt%) was dissolved in a mixture of DCM and TFE (80:20, v/v), and 10 mL of the solution was loaded into a syringe with a blunt, 23-gauge needle. The syringe was then placed in a syringe pump (KD Scientific single-syringe infusion pump, Holliston, MA, USA), and the PLLA solution was ejected into a collector at 17 kV from a high-voltage power supply (NanoNC, Seoul, Korea). The solution flow rate and spinning time were set to 1 mL h^{-1} and 10 h, respectively. Following the spinning process, the electrospun meshes were dried at room temperature for 6 h at 40 ºC overnight.

Fragmentation of the nanofibrous mesh to fibrous particles

The prepared electrospun meshes were cut into small pieces (5 × 5 mm) and were immersed in a 10 wt % of HMDA solution prepared in isopropyl alcohol (IPA), which was then shaken at 200 rpm in a shaking incubator at 37 °C (SI-600R, Jeio Tech, Korea) for 30 min. After that, the fragments were withdrawn by centrifugation at 4000 rpm (Combi-514R, Hanil Science, Korea), and vigorous washing with an excess volume of IPA and distilled water (DW) was repeated three times. We obtained the FP after freeze-drying for 24 h, and the morphology was observed using a scanning electron microscope (SEM, JSM-6300, JEOL, Japan) and optical microscope (DMI 4000B, Leica, Germany) after dispersing the sample in DW.

AAc grafting by γ-ray irradiation

AAc was grafted to the particles using irradiation with cobalt 60. Briefly, the pre-wetted FP was dispersed in AAc solutions (10 mL) at concentrations of 1, 3, and 5 wt% with 0.01 M ammonium ferrous sulphate. The AAc was then exposed to 1-10 kGy of irradiation at an ambient temperature. Unreacted monomers and homopolymers were washed away by stirring with an excess of DW for 12 h, and the AAc-grafted FP was freeze-dried. To measure the carboxyl group contents on the FP, we performed toluidine blue O (TBO) staining (4 mg toluidine blue O chloride, 0.1 M HCl, and 20 mg NaCl) for 4 h. The TBO-stained FP was suspended in a 0.1 M NaOH and ethanol solution (1: 4 v/v) until complete decolourization, and the uptake amounts of TBO were quantified by measuring the solution's absorbance at 530 nm using a plate reader (Powerwave XS, Biotek, VT, USA). A standard calibration curve was obtained using known concentrations of TBO. The surface property of the FP was also analysed using ATR-FTIR (TENSOR 37 Spectrophotometer, Bruker, Germany).

RGD peptide conjugation and quantification

The carboxyl groups of the AAc-grafted FP were activated with EDC/NHS in an MES buffer (pH 5.3) for 30 min and were sequentially immersed in 0.1-5 mM RGD peptide (CGGGRGDS, Anygen, Jangseong, Korea) solutions (10 mM sodium bicarbonate buffer, pH 8.3) with gentle shaking for 12 h. Then, the FP was washed with DW three times, and freeze-dried for 12 h to obtain RGD peptide coupled-FP powders (R-

FP). A quantitative analysis of the peptide conjugation was performed using a fluorescamine assay. A fluorescamine solution (4 mg mL^{-1}, acetone) was briefly mixed in a 0.25 M borate buffer (pH 9) with a mixing ratio of 1:9, which was then mixed with the remaining or washed solutions (mixing ratio 25:75) after peptide conjugation. After 60 s of vigorous shaking, the fluorescence from the samples was measured using a fluorescence microplate reader (390 nm of excitation and 475 nm of emission wavelength, Spectra Max M2e, Molecular Devices, CA, USA). A standard calibration curve was also obtained from the intensity of known concentrations of the RGD peptide solutions. RGD-coupled alginate was also prepared as described previously.[27] After EDC/NHS and RGD peptide reaction, the RGD-alginate was purified by dialysis (3.5 kD MWCO, Spectrum Lab, TX, USA) in DW for three days and then lyophilized. The dried product was stored in a vacuum-desiccator prior to use.

Preparation of fibrous particle-loaded hydrogels and rheological measurement

The alginate solution (2 wt%) mixed with the FP (2 and 8 mg mL^{-1}) was filled in the syringe and quickly re-mixed with a 21 wt% calcium sulphate (CaSO$_4$) slurry (alginate solution: calcium sulphate slurry = 1: 0.04). To assess the FP distribution in the hydrogel, the specimen was sectioned and observed using an optical microscope (DMI 4000B, Leica, Germany). Rheological analysis was performed as described previously.[27] The mixed solution was quickly placed on the plate, and the moduli of the hydrogel (frequency: 0.01-1 Hz) were measured using a rheometer (ARES, TA Instruments, DE, USA) equipped with a cone and plate fixture (25 mm diameter plate and 0.1 rad cone). The gelation behaviour was monitored with a single frequency mode at 1 Hz for 15 min.

Preparation of hMSC-encapsulated hydrogel disks

hMSC (PT-2501, Lonza Group Ltd., Basel, Switzerland) was homogeneously re-mixed to achieve an R-FP (8 mg mL^{-1})/cell-suspended alginate solution (2 × 10^6 cells mL^{-1}) and was cross-linked as described above. The mixed solution was placed in a sterilized glass chamber (55 × 25 × 1 mm), and then punched into disks eight mm in diameter. The hydrogel disks were incubated at 37 °C in a 5% CO$_2$ atmosphere, and the growth medium (GM, low glucose DMEM supplemented with 10% FBS and 1% penicillin/streptomycin) was changed every two days.

Cell viability analysis

To evaluate the viability of hMSC in the hydrogels, a cell counting kit (CCK-8, Dojindo, Japan) was used following the manufacturer's instructions. Briefly, the CCK-8 was mixed with medium in a 1:9 ratio and further incubated for 120 min at 37 °C. Following the reaction, the absorbance of the medium (200 μL) was recorded at 450 nm using a microplate reader (Powerwave XS, Biotek, USA). After 14 days of culture, we investigated the cell viability using a Live/Dead assay. Briefly, the specimen was incubated in a mixture 3 μM

fluorescein diacetate/ 0.5 μM ethidium bromide for 10 min and washed with PBS for 5 min, twice. The immunofluorescent images were obtained using a fluorescent microscope (DMI 4000B, Leica, Germany).

Immunofluorescent staining

The cells cultured for three days were fixed using 3.7% paraformaldehyde for 20 min. The specimens were permeabilized with a cytoskeletal buffer solution (10.3 g sucrose, 0.292 g NaCl, 0.06 g MgCl$_2$, 0.476 g HEPES buffer, 0.5 mL Triton X-100, in 100 mL water, pH 7.2) for 20 min at 4 °C and then blocked with 5% BSA in PBS for 90 min at 37°C. The fixed cells were incubated with anti-paxillin (1:100, BD science, NJ, USA) for 90 min at 37°C and were subsequently incubated with 1:50 Alexa fluor 488 rabbit anti-mouse IgG, 1:100 rhodamine-phalloidin, and 1:5000 Hoechst 33258 for 90 min at 37 °C. After washing with PBS, the samples were mounted on glass slides with a Vectashield mounting medium (Vector Laboratory, UK). To obtain the image for cell spread in 3D, we scanned the specimens every 1 μm thickness to 60-100 μm by using Z-stacking mode on a confocal laser-scanning microscope (TCS SP-5, Leica, Germany). The images were rendered for 3D imaging using Leica application suite.

Osteogenic differentiation and mineralization

To evaluate the effect of R-FP in the hydrogel on the ALP activity and mineralization of hMSC, the hydrogels were incubated within the osteogenic differentiation media (OM) supplemented with 2.84 × 10^{-4} M L-ascorbic acid, 1 × 10^{-2} M β-glycerol-phosphate and 10^{-7} M dexamethasone and cultured for seven or fourteen days. After lysis of hMSCs with the radio immunoprecipitation assay (RIPA) lysis buffer (1% Triton X-100, 0.1% SDS, 1% sodium deoxycholate, 150 mM NaCl, 150 mM Tris, pH 7.2, and protease inhibitors) and homogenization (T10 basic, IKA, Germany), the lysates were allowed to react with the ALP solution for ELISA (Sigma Aldrich, St. Louis, MO, USA) for 30 min at 37 °C. The optical density was then observed using a microplate reader at a 405 nm wavelength. The intensity of the known concentrations of the paranitrophenyl phosphate (0-600 μg mL^{-1}) was measured for a standard curve, and the total protein content from each sample was also quantified using a Micro BCA assay (Thermo Scientific, IL, USA). For Alizarin Red S (ARS) staining, the cells in the hydrogels were cultured in GM and OM for 14 days. The constructs were fixed with 4% paraformaldehyde and were subsequently stained with a 2% ARS solution (pH 4.2) for five minutes at room temperature. Following PBS washing, the ARS-stained hydrogels were homogenized, and the stained ARS was extracted from the cells with 5% SDS in 0.5 N HCl (0.5 mL) for 30 min. The absorbance of the extracted ARS was measured at 405 nm.

Statistical analysis

All data are presented as mean ± standard deviation (SD) for n=3. The statistical significance was assessed using ANOVA and a Student's t-test ($p < 0.05$).

Results and Discussion

Fragmentation of the nanofibrous meshes

Our strategy to introduce fibrous particles to the alginate hydrogel for cell adhesion is illustrated in Fig. 1. First, we prepared a PLLA nanofibrous mesh using an electrospinning method, and we fragmented the mesh using a strong basic solution under vigorous shaking. The prepared FPs were functionalized with AAc and RGD peptides, and then incorporated in the alginate hydrogel with hMSC. Previously, we reported the aminolysis of PLLA mesh with varying periodic lengths (mean length: 1.2 - 13.8 µm) by rupture at the amorphous region between the lamellar crystalline domains under shear-stress.[25] The photographic and microscopic images of PLLA mesh are shown in Fig. 2a and 2b, respectively, demonstrating an average fibre diameter of 1 µm and a random fibrous network. The electrospun mesh was fragmented into rod-shaped particles during aminolysis, and we obtained FP powder as shown in Fig. 2c and 2d. The FPs were dispersed in the DW after being wetted with 70 % ethanol, as shown in Fig. 2e and 2f, resulting in a non-transparent solution. The particle length varied from approximately 10 to 80 µm (mean length: 28.9 ± 6.6 µm), and the original diameter of the fibres was maintained due to a relatively short time of aminolysis.

AAc grafting by γ-ray irradiation and RGD peptide conjugation

The aminolysis allowed the FP to present amine and hydroxyl groups as described in Fig. 1,[28,29] and we also grafted AAc to introduce carboxyl groups by γ-ray irradiation that can be used as a bridge for peptide conjugation. Radiation-based modifications with γ-rays, electron-beams and ion-beams has been widely used to modify the property of materials.[30-32] These approaches are effective to introduce a functional group or to control the molecular weight of materials.[33] We also reported that the degree of AAc grafting by γ radiation was precisely controlled on the films and nanofibres.[34, 35] The successful graft was visualized and quantified with TBO staining as described previously.[36] TBO was remained bound to the AAc-grafted FP, even under vigorous washing, and the concentration of the carboxyl groups on the particles varied from 0.3 to 490 nmol/mg according to the grafting condition (Fig. 3a). In addition, we confirmed a new peak at 1704 cm^{-1} in the ATR-FTIR spectrum that reflected a signal from the C=O stretch of the carboxyl groups. This peak increased as the AAc amounts increased indicating successful introduction of carboxyl groups (Fig. 3b). Next, we conjugated RGD peptides

to the carboxyl groups of the FP (AAc grafted under 10 wt% AAc at 5 kGy) using EDC/NHS chemistry.

For easy conjugation of biomolecules, such as proteins or peptides, the materials should have a functional group such as a carboxyl, amine or thiol group.[37] To induce the functional group, the material was newly synthesized or the molecules with those groups were grafted by UV irradiation or plasma treatment.[38] Using the traditional methods, the induced functional group varied from pico- to nanomolar levels. Consequently, the conjugated RGD peptide was also measured at the same levels.[26,39,40] As shown in Fig 3c, the amounts of RGD on the R-FP were 7.2 ±3.7, 49.5 ±7.4, and 177.2 ±18.9 nmol mg^{-1} corresponding to the feed amounts of 0.1, 1, and 5 mM, respectively. These levels were approximately 60 times greater than those in our previous report that was performed without carboxyl groups (3 nmol mg^{-1} nanofilaments).[26] This remarkable amount of immobilization may result from of the high number of carboxyl groups induced by radiation, which suggests that these functional groups can be an acceptable cell-binding additive.

Preparation of fibrous particle-loaded hydrogels and rheological analysis

The degree of cross-linking, or stiffness of the hydrogel, is one of the determinants that regulates the fate of stem cells encapsulated within the hydrogel. For instance, stem cells within an RGD peptide-functionalized alginate hydrogel with various elastic moduli presented different gene expressions,[41] and enzyme-mediated cross-linked gelatin-PEG-tyramine hydrogel also exhibited modified cell viability according to the degree of cross-linking.[42] Moreover, some additives, such as microparticles or cells, have been loaded in hydrogels for growth factor delivery or for alternative cross-linking.[11, 43-45] Similarly, we incorporated the FP or R-FP in the hydrogel and investigated their effect on gelation or mechanical properties of the hydrogel under a constant cross-linker concentration.[27]

As shown in Fig. 4a, the alginate hydrogel was transparent as described in other reports,[46,47] and the FP-loaded hydrogel was non-transparent, which prevented recognition of the letters at the bottom of the hydrogel. Furthermore, we found that the FP was homogeneously distributed throughout the hydrogel in a cross-section image, indicating that the AAc modification by γ-ray-irradiation successfully improved the distribution of FP by increasing hydrophilicity (Fig. 4b).

The mechanical properties of the alginate hydrogel have been regulated by cross-linkers, cross-linking concentrations, or time of cross-linking, which resulted in a wide range of mechanical properties.[41,48] The increase of hydrogel modulus has also been regulated by additives, in which larger amounts of supplements augmented the mechanical property of the hydrogels.[27,49] We investigated the FP's effect on the gelation time at constant cross-linking conditions (CaSO$_4$ concentration 48 mM). As presented in Fig. 4c, storage and loss modulus of pure alginate reached equilibrium at 350 s after mixing the alginate with calcium sulphate. However, the gelation time was delayed in the FP-loaded alginate hydrogel.

When 2 mg FP was loaded, gelation was achieved at 450 s, and 8 mg of FP-containing gel required over 700 s for gelation. The increased gelation time may be due to the FP's even spatial distribution in the alginate solution. As shown in Fig. 4b, the widely dispersed FP may interfere with the combination of the alginate chain with calcium ions. Furthermore, because the introduced carboxyl groups on the FP can bind calcium ions,[50] a relatively slow gelation may result. To investigate the mechanical property of the hydrogel, we cross-linked the hydrogel for 30 min and then measured modulus using a rheometer. The storage modulus of the alginate hydrogel has been reported to range from 1 to 5 kPa,[46,51,52] and we also obtained a similar storage modulus (4.82 kPa) of 1 Hz frequency. As FP was loaded in the gel, the storage modulus significantly increased to 6.92 and 21.68 kPa in the 2 mg and 8 mg FP-loaded groups, respectively. As described previously, the additives may affect the property of alginate hydrogel, depending on their participation in cross-linking or support of the overall mechanical load.

In our study, a similar enhancement of mechanical property was observed, which might be due to the intrinsic property and shape of the PLLA-based FP. PLLA has been known to be a brittle material with a 200 MPa elastic modulus (as an electrospun nanofiber).[53] Even though FP was generated by aminolysis and partial degradation, the rigidity of FP seems to have a significantly greater modulus than the pure hydrogel. Furthermore, the elongated shape of FP might provide the rigid property of the hydrogel, resulting in a higher modulus than pure hydrogel. However, the enhanced modulus of the FP-loaded hydrogel seems to result at a macroscopic level, while a hydrogel region without FP may exhibit a similar modulus to that of pure alginate hydrogel.

Viability of 3D-encapsulated hMSCs within the hydrogels

Several bioactive molecules guide the biological responses of cells by receptor- or integrin-mediated signalling. In particular, the RGD peptide has been shown to regulate cell adhesion, spreading on the substrates, and a series of prolonged behaviours such as proliferation or differentiation.[21-23] To find the biological function of the R-FP incorporated hydrogel, we encapsulated the hMSC in the hydrogel and measured cell viability for 14 days. Cytotoxicity of R-FP itself was investigated in a previous study, in which the R-FP did not showed any harmful effect up to 300 μg mL^{-1}.[26] Therefore, we did not consider the cytotoxicity of the R-FP in this study.

Previously, 3D-encapsulated hMSC in the alginate hydrogel survived well, with increased viability in the RGD peptide-conjugated alginate hydrogel due to guidance of integrin binding.[8] As shown in Fig. 5a, even though the hydrogel disks contained the same number of cells (2×10^6 cells mL^{-1}), the metabolic activity was different. The RGD-conjugated alginate (R-ALG) and the R-FP-loaded alginate hydrogel (RF-ALG) exhibited approximately two times higher cell viability even at day one. This cell viability trend was

prolonged until day 14. R-ALG and RF-ALG supported the viability of encapsulated cells, whereas the non-modified FP loaded-hydrogel (F-ALG) did not increase cell viability, similar to the pure hydrogel. In particular, the cell viability in F-ALG looks lower than that in the ALG. However, it was not statistically significant during several times of experiments. Therefore, we thought that FP itself did not affect the cell viability in the hydrogel.

The viability of encapsulated cells was also assessed by the Live/Dead assay. Most of the cells in the alginate hydrogel survived over seven days.[54] In our study, the encapsulated cells survived in the hydrogel for the initial three days, and we did not find significant differences among the groups. However, during the later incubation period, up to 14 days, dead cells were frequently observed in the ALG, F-ALG, and R-ALG groups, while only a few dead cells were found in the RF-ALG group (Fig. 5b). Furthermore, the loading amount of R-FP was significant in regulating the viability of the cells. Higher contents of R-FP (8 mg) significantly increased cell viability until day seven, compared to the hydrogel containing 2 mg R-FP (data not shown). Despite the higher modulus of the RF-ALG hydrogels, the incorporated R-FP might support cell survival for a longer time than those in the alginate hydrogel. Therefore, we found that the encapsulated cells can bind to the nearest R-FP in the hydrogels and that their binding might improve cell viability.

Spatial spreading of hMSCs

We then investigated whether binding between the cell and R-FP can modulate cell spreading in the 3D microenvironment, using confocal microscopic analysis. In the alginate hydrogels, spatial spreading morphology of the encapsulated cells was hardly observed due to the higher mechanical property or highly compact polymeric chain network, compared to those under normal cell culture conditions, in which the cells maintained a spherical shape, exhibiting only partial filopodia formation.[55] Even when collagen was mixed with alginate, a highly restricted spreading morphology was observed after in situ cross-linking.[56] In addition, the cells within the RGD-conjugated alginate hydrogel presented a slight extension of actin protrusion throughout the entire range of the elastic modulus, from 5 to 110 kPa.[8, 41]

As described in the previous reports, the cells in the alginate hydrogels still exhibited a spherical morphology similar to that of suspended cells (Fig. 6a).[8, 11, 27] We did not find polygonally spread cells, even in the R-ALG hydrogel. However, not all cells were bound to the FP or R-FP, and some cells undoubtedly bound with the FP or R-FP, presenting both an anisotropic and polygonal shape in 3D. It was very hard to measure the extent of cell spreading (length, aspect ratio) due to out-focusing and spreading on imaging. At least 20% of cells may alter their shape in the RF-ALG. Fig. 6b describes the number of particles bound to the cell. Three R-FPs revealed by numbers were involved in spatial spreading as well as morphological changes of cells. R-FP (1 and 1') of 150

µm length mainly anchored the cell from top to bottom while two short R-FPs (2 and 3) bound to filopodial projections in Z-axis. Spatial spreading of cells through R-FPs has been shown in supporting movie. Taken together R-FPs binding to cells seemed to regulate 3D cell spreading, which may promote prolonged cell survival by mimicking the function of collagen fibrils as discussed earlier.

Osteogenic differentiation and mineralization

Because we confirmed that the RF-ALG hydrogel partially promoted spatial spreading and enhanced viability of cells in the 3D environment, we proceeded to examine the effect of R-FP on differentiation. Previously, RGD-functionalized nanofiber meshes and alginate hydrogel facilitated the osteogenic differentiation and mineralization of hMSCs.[35, 57] Since our system can concomitantly provide biological (RGD motif) and structural (nanofibrous structure) signals, we expected that differentiation could be improved. After induction of osteogenic differentiation, we measured alkaline phosphatase (ALP) activity as an osteogenic differentiation marker (Fig. 7a). ALP activity was 9.9 ± 0.6 nmol min^{-1} mg^{-1} protein in the RF-ALG hydrogels, which were approximately 1.6-, 1.9- and 2.1-times greater than those from ALG (6.1 ± 0.3 nmol min^{-1} mg^{-1} protein), R-ALG (5.2 ± 1.5 nmol min^{-1} mg^{-1} protein), and F-ALG (4.6 ± 0.5 nmol min^{-1} mg^{-1} protein), respectively, after one week of induction. Furthermore, ALP activity in all groups increased after two weeks, with RF-ALG inducing the most ALP activity (13.6 ± 0.3 nmol min^{-1} mg^{-1} protein). The enhanced activity was at a similar level to that of the R-ALG group (14.5 ± 0.7 nmol min^{-1} mg^{-1} protein), which was still greater than those in the ALG (11.6 ± 0.3 nmol min^{-1} mg^{-1} protein) and F-ALG groups (10.7 ± 0.4 nmol min^{-1} mg^{-1} protein), indicating that incorporated R-FP can facilitate or improve the late cell responses by binding to the R-FP.

An assessment of mineralization was conducted using ARS staining. As shown in Fig. 7b, the degree of ARS uptake was lower in the GM culture than in the OM culture, which suggests that mineralization might be restricted because of the absence of mineralization inducing signals. Quantitative analysis of mineralization was calculated by subtracting the measured OD values of ARS extracts from those of the hydrogels cultured in OM or GM. Mineralization was significantly increased in the R-ALG and RF-ALG hydrogels. The ALG and F-ALG hydrogels exhibited only half the value of ARS, while R-ALG and RF-ALG hydrogels exhibited values that were three times higher, indicating that the RGD peptide coupled to the alginate or the FP successfully triggered mineralization, even in the 3D microenvironment (Fig. 7c). ARS positive cells were frequently observed in the R-ALG and RF-ALG hydrogels, whereas the ALG and F-ALG hydrogels only partially exhibited red-stained cells (Fig. 7d). Consequently, R-FP loaded hydrogels might offer a proper cell-binding site on the cell-adhesive peptides of the fibrous particles, which may also confer guidance for differentiation and mineralization of the 3D encapsulated cells.

Conclusions

In this report, we developed a hybrid hydrogel to concomitantly present structural and biochemical cues for regulating proliferation, spatial spreading, and osteogenic differentiation of 3D-encapsulated hMSCs. The fibrous particles, functioning as cell anchorage sites, were prepared by aminolysis of electrospun PLLA meshes, which were functionalized with AAc and RGD peptides by γ-ray irradiation and common EDC/NHS chemistry. The RGD-coupled fibrous particles can be easily incorporated into alginate hydrogels, in which they can bind to the cells resulting in remarkable cell regulation in a novel 3D microenvironment. The current hydrogel system for cell delivery has failed to play a fundamental role as an artificial ECM due to absence of cell-binding motif and structural difference. As a next generation hydrogel, our hybrid system with fibrous particles provides the general properties of raw materials as well as a fibrous anchorage site, which is not present in the previous hydrogel system. In addition, this approach can not only be applied to the alginate but can also be utilized in a variety of hydrogels, such as hyaluronic acid, gelatin, and PEG hydrogels, for developing new hydrogel systems in tissue engineering applications. Therefore, our strategy to append the fibrous particles to the hydrogel can be used as an alternative tool to improve the survival of 3D-encapsulated cells and the regeneration of damaged tissue.

Acknowledgements

Notes and references

[a] Research Division for Industry & Environment, Advanced Radiation Technology Institute, Korea Atomic Energy Research Institute, 29 Gumgugil, Jeongeup 580-185, Korea

[b] Severance Hospital Integrative Research Institute for Cerebral & Cardiovascular Diseases (SIRIC), Yonsei University Health System, 50 Yonsei-ro, Seodaemun-gu, Seoul 120-752, Korea

[c] Department of Bioengineering, College of Engineering, Hanyang University, 222 Wangsimni-ro, Seongdong-gu, Seoul 133-791, Korea

[d] Department of Internal Medicine, College of Medicine, Hanyang University, 222 Wangsimni-ro, Seongdong-gu, Seoul 133-791, Korea

[e] School of Materials science and Engineering, Gwangju Institute of Science and Technology, Gwangju 500-712, Korea

*Corresponding author: Dr. Youn-Mook Lim
Email: ymlim71@kaeri.re.kr
Phone number: +82-63-570-3065
Fax: +82-63-570-3069

1. J. L. Drury and D. J. Mooney, *Biomaterials*, 2003, **24**, 4337-4351.
2. K. B. Fonseca, F. R. Maia, F. A. Cruz, D. Andrade, M. A. Juliano, P. L. Granja and C. C. Barrias, *Soft Matter*, 2013, **9**, 3283-3292.
3. F. Topuz, A. Henke, W. Richtering and J. Groll, *Soft Matter*, 2012, **8**, 4877-4881.
4. H. Zimmermann, F. Wählisch, C. Baier, M. Westhoff, R. Reuss, D. Zimmermann, M. Behringer, F. Ehrhart, A. Katsen-Globa, C. Giese, U. Marx, V. L. Sukhorukov, J. A. Vásquez, P. Jakob, S. G. Shirley and U. Zimmermann, *Biomaterials*, 2007, **28**, 1327-1345.
5. S. Duggal, K. B. Frønsdal, K. Szöke, A. Shahdadfar, J. E. Melvik and J. E. Brinchmann, *Tissue eng.*, 2009, **15**, 1763-1773.
6. J. Tritz, R. Rahouadj, N. de Isla, N. Charif, A. Pinzano, D. Mainard, D. Bensoussan, P. Netter, J.-F. Stoltz, N. Benkirane-Jessel and C. Huselstein, *Soft Matter*, 2010, **6**, 5165-5174.
7. S. l. J. Bidarra, C. C. Barrias, M. r. A. Barbosa, R. Soares and P. L. Granja, *Biomacromolecules*, 2010, **11**, 1956-1964.
8. S.-W. Kang, B.-H. Cha, H. Park, K.-S. Park, K. Y. Lee and S.-H. Lee, *Macromol. Biosci.*, 2011, **11**, 673-679.
9. X. Liu, W. Peng, Y. Wang, M. Zhu, T. Sun, Q. Peng, Y. Zeng, B. Feng, X. Lu, J. Weng and J. Wang, *J. Mater. Chem. B*, 2013, **1**, 4484-4492.
10. B. Sarker, D. G. Papageorgiou, R. Silva, T. Zehnder, F. Gul-E-Noor, M. Bertmer, J. Kaschta, K. Chrissafis, R. Detsch and A. R. Boccaccini, *J Mater. Chem. B*, 2014, **2**, 1470-1482.
11. H.-j. Lee, S.-H. Ahn and G. H. Kim, *Chem. Mater.*, 2011, **24**, 881-891.
12. R. M. S. Nicola C. Hunt, Deborah J. Henderson, and Liam M. Grover., *Tissue eng.*, 2013, **19**, 905-914.
13. B.-H. Lee, B. Li and S. A. Guelcher, *Acta Biomater.*, 2012, **8**, 1693-1702.
14. M. Shachar, O. Tsur-Gang, T. Dvir, J. Leor and S. Cohen, *Acta Biomater.*, 2011, **7**, 152-162.
15. A. Goren, N. Dahan, E. Goren, L. Baruch and M. Machluf, *FASEB J.*, 2010, **24**, 22-31.
16. J.-S. Yang, Y.-J. Xie and W. He, *Carbohydr. Polym.*, 2011, **84**, 33-39.
17. C. Frantz, K. M. Stewart and V. M. Weaver, *J. Cell Sci.*, 2010, **123**, 4195-4200.
18. H. Fernandes, L. Moroni, C. van Blitterswijk and J. de Boer, *J. Mater. Chem.*, 2009, **19**, 5474-5484.
19. S.-C. Wu, W.-H. Chang, G.-C. Dong, K.-Y. Chen, Y.-S. Chen and C.-H. Yao, *J. Bioact. Compat. Polym.*, 2011, **26**, 565-577.
20. T. J. Sill and H. A. von Recum, *Biomaterials*, 2008, **29**, 1989-2006.
21. Y. M. Shin, J.-Y. Lim, J.-S. Park, H.-J. Gwon, S. Jeong and Y.-M. Lim, *Biotechnol. Bioprocess Eng.*, 2014, **19**, 118-125.
22. J. Xie, X. Li, J. Lipner, C. N. Manning, A. G. Schwartz, S. Thomopoulos and Y. Xia, *Nanoscale*, 2010, **2**, 923-926.
23. S. I. Jeong. J.B. Lee, M.S. Bae, D.H. Yang, D.N. Heo, C.H. Kim, E. Alsberg, I.K. Kwon, *Tissue eng.*, 2011, **17**, 2695-2702.
24. Q. P. Pham, U. Sharma and A. G. Mikos, *Biomacromolecules*, 2006, **7**, 2796-2805.
25. T. G. Kim and T. G. Park, *Macromol. Rapid Commun.*, 2008, **29**, 1231-1236.
26. T. G. Kim, S.-H. Park, H. J. Chung, D.-Y. Yang and T. G. Park, *Adv. Funct. Mater.*, 2010, **20**, 2303-2309.
27. H. Park, S.-W. Kang, B.-S. Kim, D. J. Mooney and K. Y. Lee, *Macromol. Biosci.*, 2009, **9**, 895-901.
28. Y. Zhu, Z. Mao and C. Gao, *RSC Adv.*, 2013, **3**, 2509-2519.
29. C. G. Yabin Zhu, Xingyu Liu, Tao He, Jiacong Shen, *Tissue eng.*, 2004, **10**, 53-61.
30. I.-T. Hwang, M.-Y. Ahn, C.-H. Jung, J.-H. Choi and K. Shin, *J. Biomed. Nanotech.*, 2013, **9**, 819-824.
31. X. Ping, M. Wang and G. Xuewu, *Rad. Phys. Chem.*, 2011, **80**, 567-572.
32. A. Schulze, M. F. Maitz, R. Zimmermann, B. Marquardt, M. Fischer, C. Werner, M. Went and I. Thomas, *RSC Adv.*, 2013, **3**, 22518-22526.
33. Deelder, O. Güven, H. Ha, E.-S. Hegazy, A. S. Hoffman, I. Kaetsu, R. O. Mazzei, Z. Nurkeeva, M. T. Razzak, J. M. Rosiak, A. Safrany and M. Sen, *Radiation Synthesis and Modification of Polymers for Biomedical Applications*, IAEA, 2003.
34. Y. M. Shin, K. S. Kim, Y. M. Lim, Y. C. Nho and H. Shin, *Biomacromolecules*, 2008, **9**, 1772-1781.
35. Y. M. Shin, H. Shin and Y. Lim, *Macromol. Res.*, 2010, **18**, 472-481.
36. L. Grøndahl, A. Chandler-Temple and M. Trau, *Biomacromolecules*, 2005, **6**, 2197-2203.
37. A. de Mel, G. Jell, M. M. Stevens and A. M. Seifalian, *Biomacromolecules*, 2008, **9**, 2969-2979.
38. G. Delaittre, A. M. Greiner, T. Pauloehrl, M. Bastmeyer and C. Barner-Kowollik, *Soft Matter*, 2012, **8**, 7323-7347.
39. M.-H. Ho, L.-T. Hou, C.-Y. Tu, H.-J. Hsieh, J.-Y. Lai, W.-J. Chen and D.-M. Wang, *Macromol. Biosci.*, 2006, **6**, 90-98.
40. T.G. Kim, T.G. Park, *Tissue eng.*, 2006, **12**, 221-233.
41. N. Huebsch, P. R. Arany, A. S. Mao, D. Shvartsman, O. A. Ali, S. A. Bencherif, J. Rivera-Feliciano and D. J. Mooney, *Nat. mater.*, 2010, **9**, 518-526.
42. K. M. Park, K. S. Ko, Y. K. Joung, H. Shin and K. D. Park, *J. Mater. Chem.*, 2011, **21**, 13180-13187.
43. H. W. Michelle T. Poldervaart, Johan van der Stok, Harrie Weinans, Sander C. G. Leeuwenburgh, F. Cumhur Öner, Wouter J. A. Dhert, and Jacqueline Alblas, *PLoS One*, 2013, **8**, e72610.
44. H. Park and K. Y. Lee, *Carbohydr. Polym.*, 2011, **86**, 1107-1112.
45. J. Lee and K. Y. Lee, *Macromol. Biosci.*, 2009, **9**, 671-676.
46. C. K. Kuo and P. X. Ma, *Biomaterials*, 2001, **22**, 511-521.
47. W. Song, A. C. Lima and J. F. Mano, *Soft Matter*, 2010, **6**, 5868-5871.
48. A. Banerjee, M. Arha, S. Choudhary, R. S. Ashton, S. R. Bhatia, D. V. Schaffer and R. S. Kane, *Biomaterials*, 2009, **30**, 4695-4699.
49. J. Fan, Z. Shi, M. Lian, H. Li and J. Yin, *J. Mater. Chem. A*, 2013, **1**, 7433-7443.
50. T. Yokoi, M. Kawashita and C. Ohtsuki, *J. Asian Ceram. Soc.*, 2013, **1**, 155-162.
51. J.-Y. Sun, X. Zhao, W. R. K. Illeperuma, O. Chaudhuri, K. H. Oh, D. J. Mooney, J. J. Vlassak and Z. Suo, *Nature*, 2012, **489**, 133-136.
52. E. R. West, M. Xu, T. K. Woodruff and L. D. Shea, *Biomaterials*, 2007, **28**, 4439-4448.
53. M. Moffa, A. Polini, A. G. Sciancalepore, L. Persano, E. Mele, L. G. Passione, G. Potente and D. Pisignano, *Soft Matter*, 2013, **9**, 5529-5539.
54. O. Jeon and E. Alsberg, *Tissue eng.*, 2013, **19**, 1424-1432.
55. W. H. Tan and S. Takeuchi, *Adv. Mater.*, 2007, **19**, 2696-2701.
56. B. M. Gillette, J. A. Jensen, M. Wang, J. Tchao and S. K. Sia, *Adv. Mater.*, 2010, **22**, 686-691.
57. E. Alsberg, K. W. Anderson, A. Albeiruti, R. T. Franceschi and D. J. Mooney, *J. Dent. Res.*, 2001, **80**, 2025-2029.

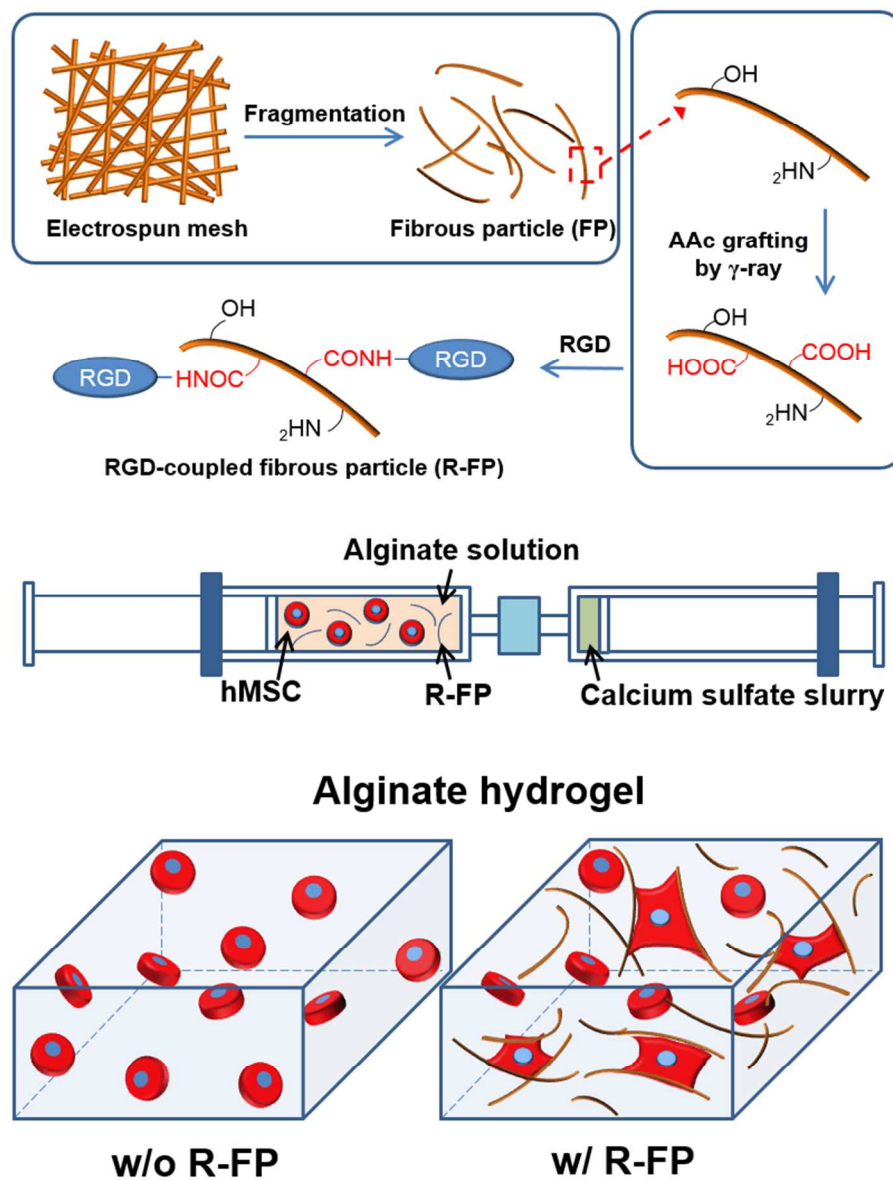*Journal of Materials Chemistry B Accepted Manuscript*

Fig. 1. Schematic diagram of the fibrous particle preparation and hMSC/fibrous particle-incorporated hydrogels
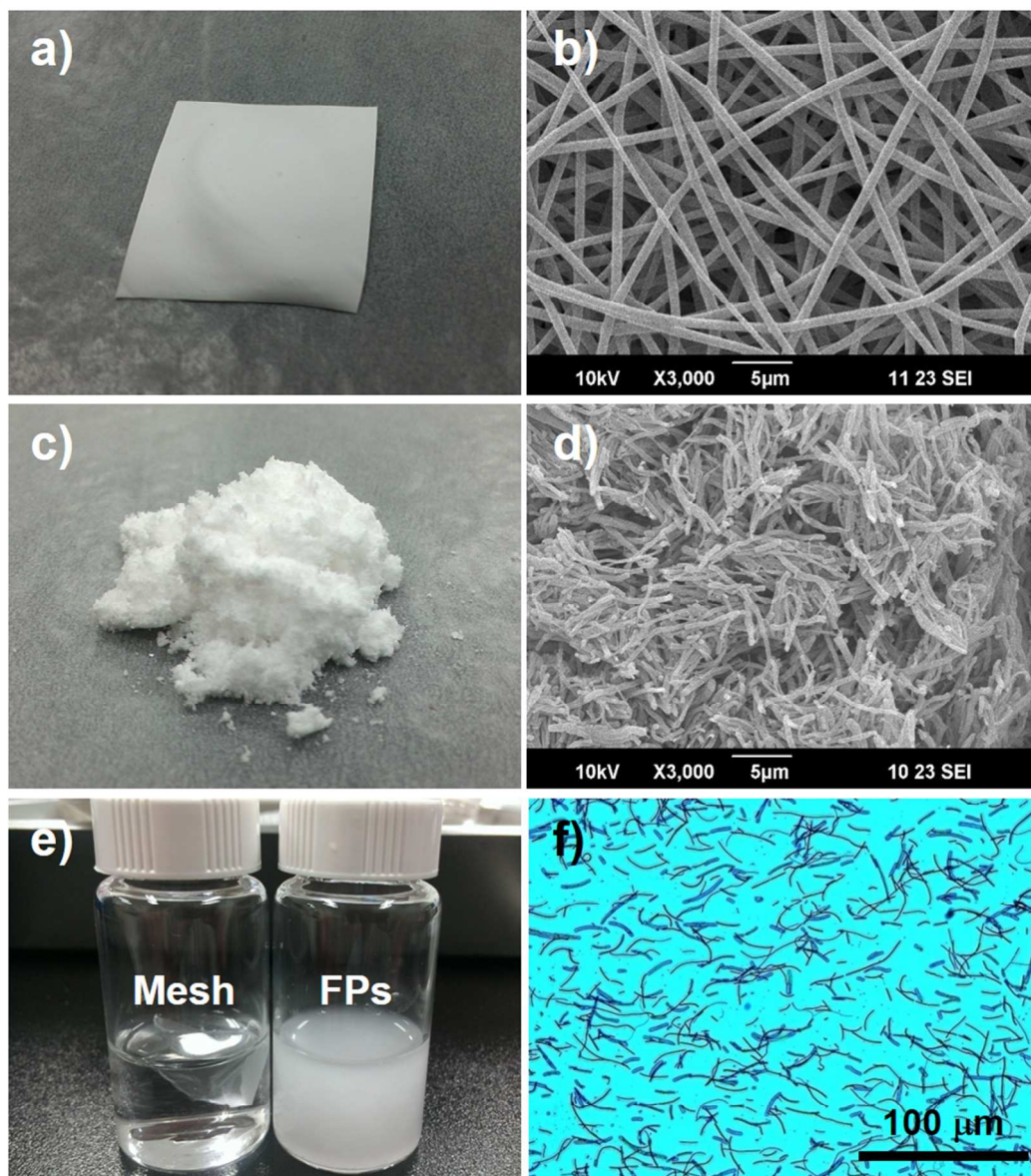
Fig. 2. Fragmentation of the electrospun meshes. a) electrospun PLLA mesh, b) scanning electron microscopy of the mesh, c) fragmented fibrous particle powder, d) scanning electron microscopy of the fibrous particle, e) dispersion of the fibrous particles in water, and f) microscopic image of the fibrous particles suspended in water
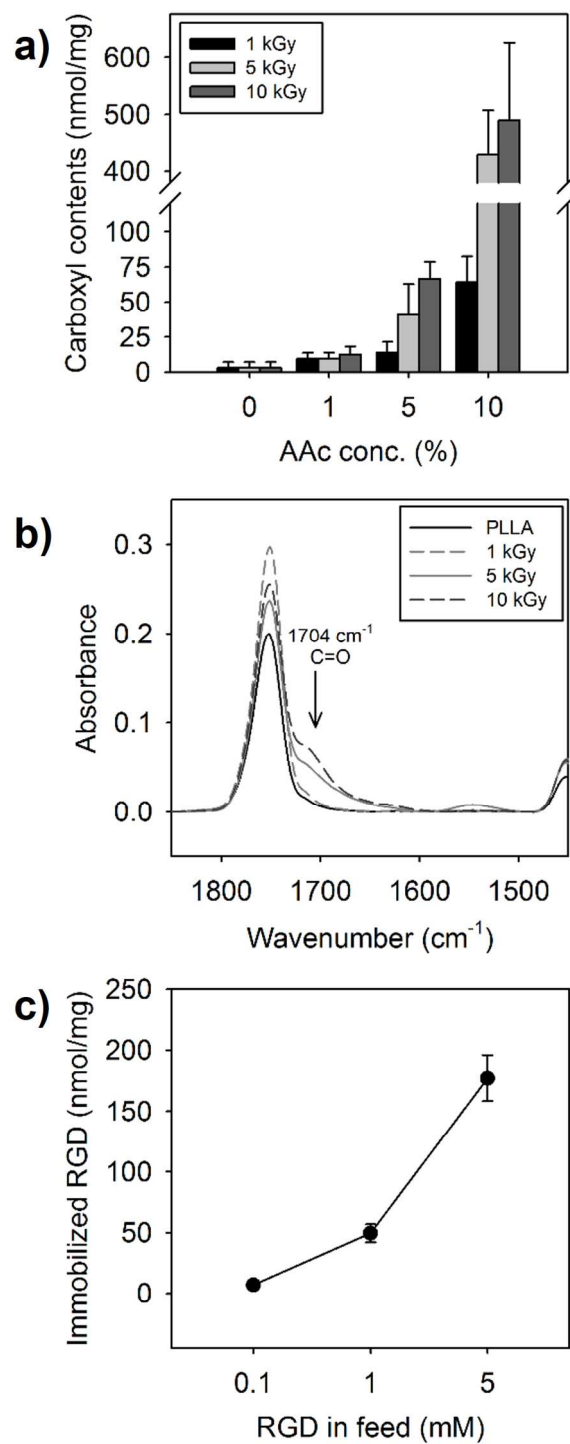
Fig. 3. Characteristics of the functionalized fibrous particles. a) quantification of carboxyl groups induced by γ-ray irradiation, b) ATR-FTIR spectrum of AAc-grafted fibrous particles (10 wt% AAc), and c) quantitative analysis of RGD peptide immobilization
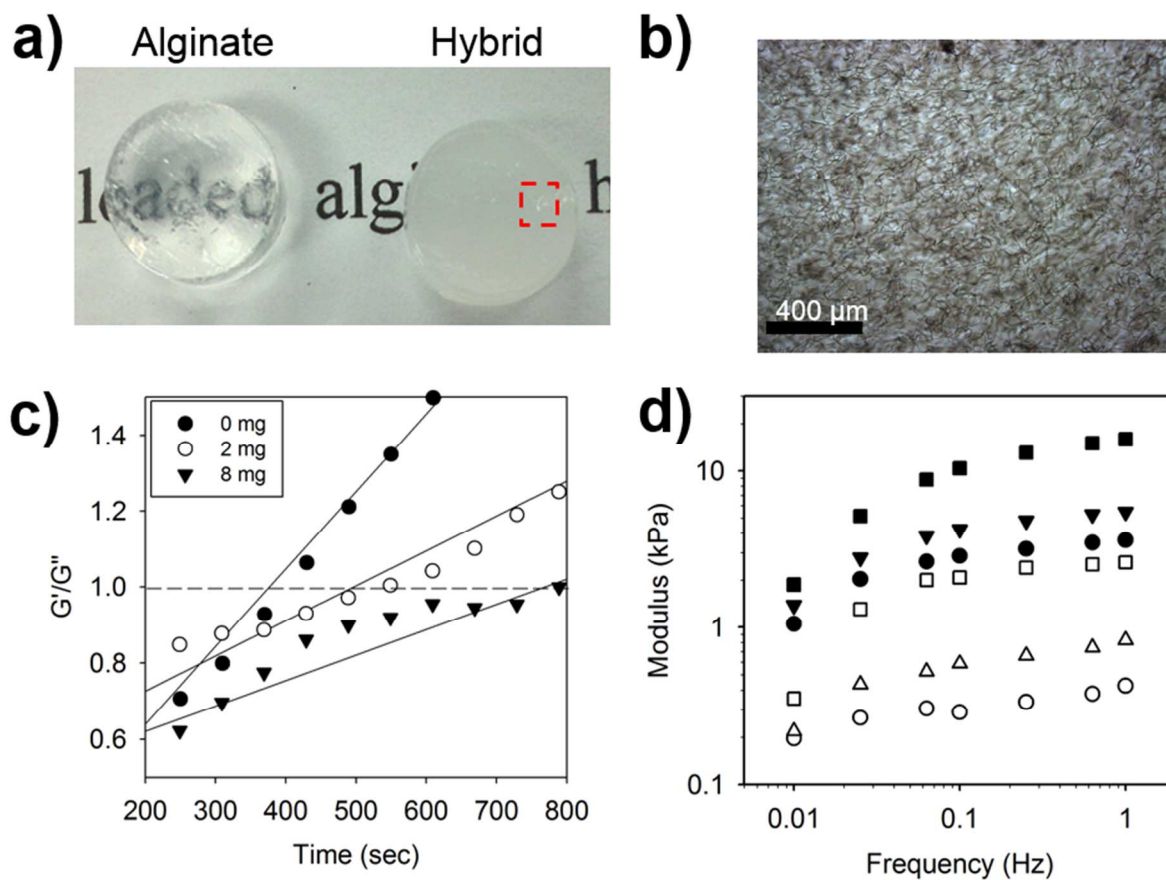
Fig. 4. Fibrous particle-loaded alginate hydrogels. a) transparency of hydrogels (red dot-line box indicates magnified area for observing FP distribution), b) distribution of FP in the hydrogel, c) gelation behaviour of hydrogels with different amounts of FP, and d) modulus of hydrogels with different FP amount (circle: 0 mg, triangle: 2 mg, square: 8 mg, filled: storage modulus, opened: loss modulus).
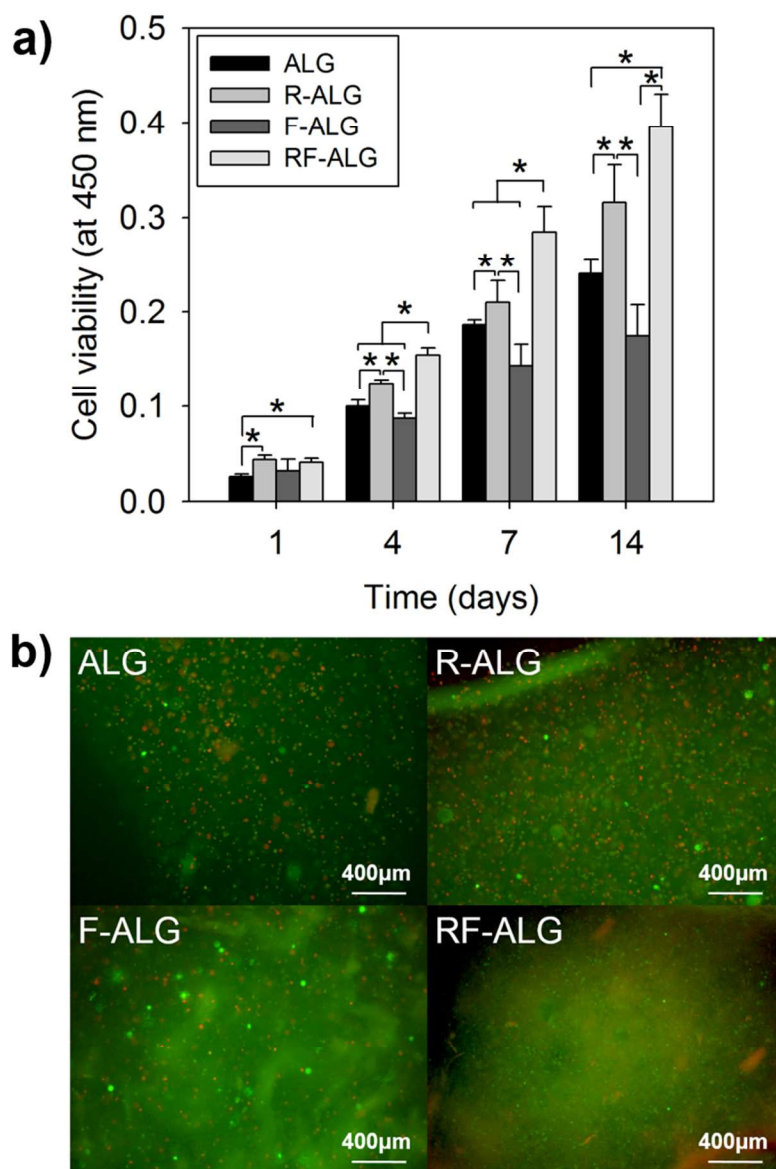
Fig. 5. Viability of hMSCs encapsulated in hydrogels. a) CCK assay for 14 days (* :$p < 0.05$), and b) Live/Dead assay at day 14 (red: dead cells-ethidium bromide, green: live cells-fluorescein diacetate)
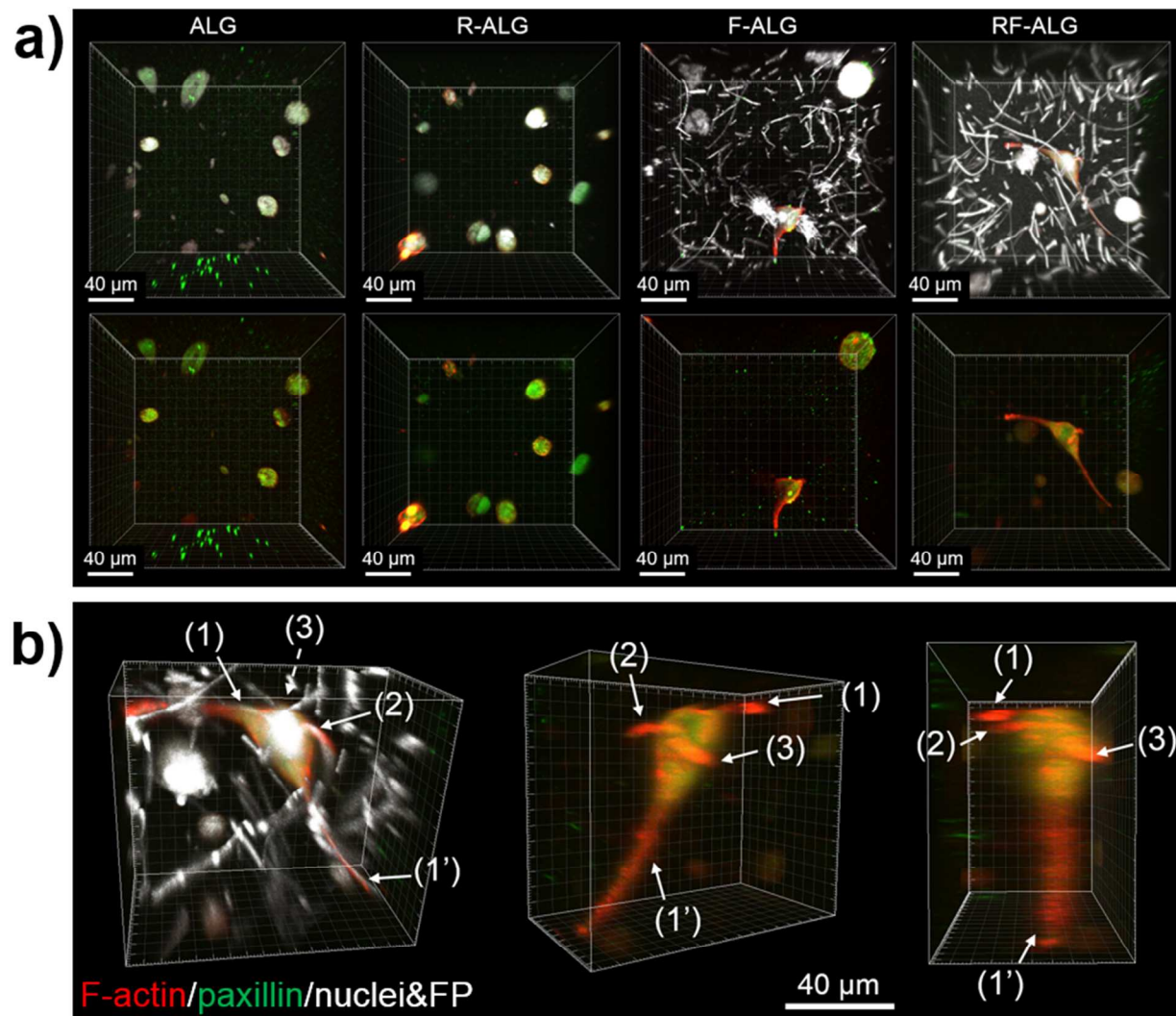
Fig. 6. Fluorescent images of the 3D-encapsulated cells in hydrogels. a) spreading morphology at day 3 by confocal laser scanning microscopy (top panel contains white: nuclei/FP, red: F-actin, and green: paxillin, whereas bottom panel excludes white signal), and b) high-magnified cell images in RF-ALG hydrogel at different view angles. The number refers to R-FP bound to cell resulting in morphological change.
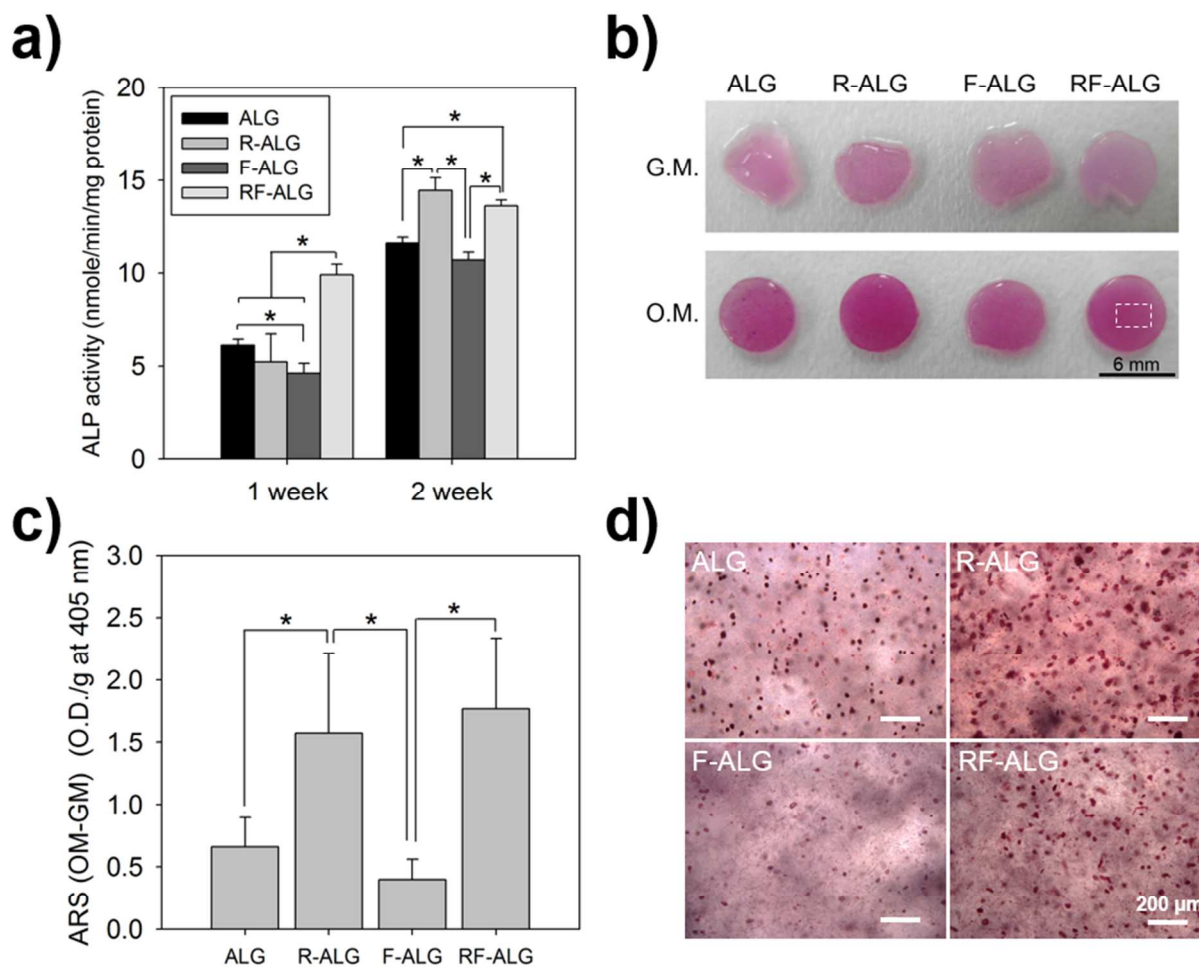
Fig. 7. Osteogenic differentiation and mineralization of encapsulated hMSC in hydrogels. a) ALP activity (*:$p < 0.05$), and b) ARS stained hydrogels under growth medium (GM) and osteogenic differentiation medium (OM) after 14 days (dot-line box indicates Fig. 7d), c) quantification of extracted ARS from the hydrogels (*:$p < 0.05$), and d) ARS-stained cells dispersed in hydrogels.

Table of contents
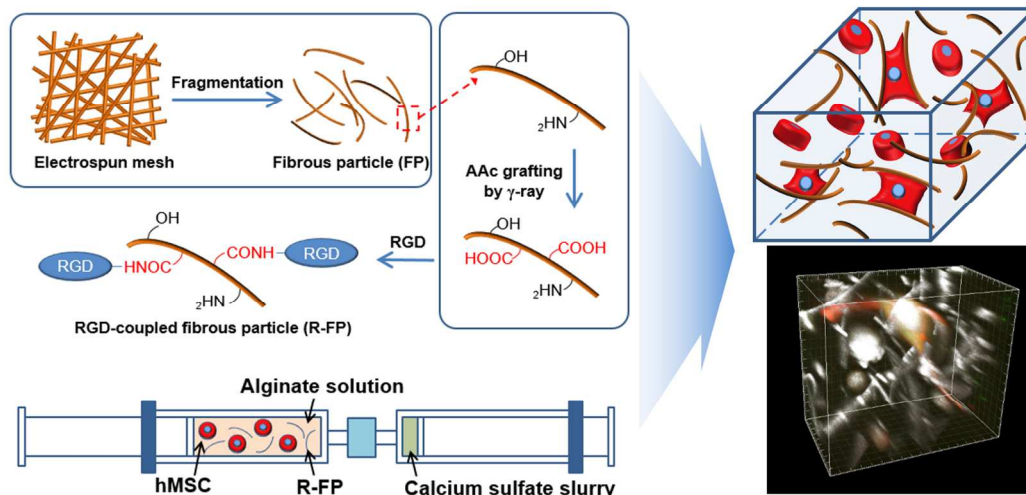
The incorporation of RGD-coupled fibrous particles to the alginate hydrogel promotes the 3D encapsulated cell behaviours by allowing the mutual binding with the particles.